Analytical and Bioanalytical Chemistry
https://doi.org/10.1007/s00216-021-03582-3

RESEARCH PAPER

Ultrasensitive zero-background photoelectrochemical biosensor for analysis of organophosphorus pesticide based on in situ formation of DNA-templated Ag_2S photoactive materials

Zhiyao Zeng[1] · Juan Tang[1,2] · Ming Zhang[1] · Shouzhi Pu[2] · Dianping Tang[3]

Received: 26 May 2021 / Revised: 24 July 2021 / Accepted: 27 July 2021

Abstract

Herein, a novel signal-on photoelectrochemical (PEC) biosensor with nearly zero background noise (ZBN) was first fabricated to determine the presence of organophosphorus pesticide based on in situ formation of DNA-templated Ag_2S photoactive materials, accompanied by hybridization chain reaction (HCR) signal amplification. The capture probe (S1) on the gold nanoparticle-modified electrode can hybridize with the aptamer molecule to generate a simple PEC biosensor. In the presence of a target molecule, the aptamer molecule is released on the double-stranded DNA (dsDNA)-modified PEC biosensor. Meanwhile, the capture probe remains on the electrode and can open the DNA hairpins (H1, H2) which are rich in cytosine, to trigger the HCR reaction. The rich "C" strands are uncovered after formation of a long dsDNA polymer strand, which can assemble multiple silver ions (Ag^+) by means of by C–Ag^+–C chelation. Then, a large number of Ag_2S can be generated by challenging with S^{2-} solution, producing a satisfactory photocurrent signal. The photoactive material is formed in situ, which eliminates the laborious operation. Moreover, the signal can be highly amplified with nearly zero background noise and HCR signal amplification. Under optimal conditions, the ZBN aptasensor exhibited high sensitivity and selectivity, with a low detection limit of 2 pg mL^{-1} for malathion. Importantly, the sensing platform can also be applied to determine the presence of malathion in real samples.

Keywords Photoelectrochemical aptasensor · Zero background · Malathion · Ag_2S · Hybridization chain reaction

Introduction

Organophosphorus pesticides (OPs), as the most commonly used group of pesticides, are indispensable substances in agriculture to ensure high crop production, owing to their low persistence and high effectiveness [1–3]. However, the mass application of OPs has caused serious public health concerns [4, 5]. It has been reported that the high toxicity of OPs is related to their ability to irreversibly inhibit the catalytic activity of acetylcholinesterase, a crucial central nervous system enzyme, causing neuromuscular paralysis and organ failure. The development of a reliable and sensitive strategy for efficient detection of OPs has thus become a global necessity [6]. Various analytical methods have been designed for the determination of OPs including high-performance liquid chromatography [7], gas chromatography-mass spectrometry [8], thin-layer chromatography [9], and liquid chromatography-tandem mass spectrometry [10]. Despite the satisfactory performance of the classical technique, it possesses some intrinsic limitations such as heavy reliance on professional staff and sophisticated instrumentation. Thus, a simple and effective strategy is needed for OP determination.

Photoelectrochemical (PEC) bioassay, an innovative analytical method, has attracted great interest due to the distinct advantages of high sensitivity, simple instrumentation, and easy miniaturization [11]. Additionally, in comparison with the classical electrochemical bioassay, the sensitivity of the PEC bioassay is greatly improved due to the lower

✉ Juan Tang
Juan_tang@hotmail.com; tjhere@126.com

[1] Key Laboratory for Green Chemistry of Jiangxi Province, Key Laboratory of Functional Small Molecules for Ministry of Education, Jiangxi Normal University, 99 Ziyang Avenue, Nanchang 330022, Jiangxi, People's Republic of China

[2] Jiangxi Key Laboratory of Organic Chemistry, Nanchang 330013, Jiangxi, People's Republic of China

[3] Key Laboratory of Analysis and Detection for Food Safety (Ministry of Education of China and Fujian Province), Department of Chemistry, Fuzhou University, Fuzhou 350108, Fujian, People's Republic of China

Published online: 10 August 2021

undesirable background noise [12–14]. Notably, photoactive materials that generate a photocurrent play a vital role in the construction of the PEC sensing platform. To date, various types of photoelectric materials have been designed and applied for fabrication of PEC bioassays, including TiO_2, CdS, $BiVO_4$, graphene, and co-sensitized structures [15–19]. Our group recently constructed a signal-on PEC sensing platform for the detection of ochratoxin A based on decahedral Au–$BiVO_4$@MoS_2 as the photoactive material [20]. Results indicated that the sensing performance was significantly improved by the co-sensitized system and the in situ-generated polyaniline wire enwrapped on the long linear DNA polymeric skeleton. However, the signal amplification was still limited because the photoactive material was directly modified on the electrode, causing high background signal [21]. Thus, a signal transduction mechanism with reduced background noise was still needed for the PEC platform.

Recently, a signal transduction mode with zero background noise (ZBN) was proposed for designing a high-efficiency ZBN PEC biosensing platform for detection of vascular endothelial growth factor [22], protein kinase A activity [23], and miroRNA14 [24]. The introduction of suitable photoactive materials with high photoelectric conversion efficiency significantly improved the sensitivity of the ZBN PEC biosensor, because it was located far from the surface of the electrode. Silver sulfide (Ag_2S), with a narrow direct band gap and wide absorption spectrum (nearly the whole visible region), is a suitable candidate for construction of a high-efficiency ZBN PEC biosensor [25, 26]. A number of methods have recently been applied for the synthesis of various kinds of Ag_2S, including microwave-activated synthesis [27], direct aqueous synthesis [28], an oil phase-based high-temperature route [29], and reverse microemulsion [30]. Despite satisfactory results of these strategies, there are still some limitations. For example, (i) synthetic nanoparticles also involve high-temperature conditions, a large amount of stabilizing agent or heavy synthesis; (ii) the photocurrent signal may decrease after labelling with biomolecules (antibody or DNA); and (iii) the morphology and the performance of the nanomaterials may change after a long period of storage. Thus, exploration of an alternative method based on photoactive materials generated in situ would be advantageous.

Signal amplification is important for constructing a sensitive ZBN photoelectrochemical biosensor. Hybridization chain reaction (HCR), a significant discovery in DNA nanotechnology, has attracted enormous interest due to its isothermal amplification and enzyme-free polymerization [31, 32]. A long double-stranded (ds)DNA product can be formed by the DNA polymerization process between two metastable DNA hairpins triggered by an initiator. It has been reported that a long dsDNA polymer can act as a scaffold for loading multiple enzymes [33], nano-catalysts [34], signal molecules [35], metal ions [36], and photoactive materials [37]. Moreover, single-stranded DNA fragments on a long dsDNA polymer can be used as a template for synthesizing nanoparticles. In this contribution, we propose a simple ZBN PEC biosensing platform to enable the sensitive detection of OPs based on in situ formation of DNA-templated Ag_2S photoactive materials. As designed, the target molecule can open the hairpin probe (H1, H2) which is rich in cytosine, to promote the HCR reaction. Thus, the rich "C" strands on the hairpin probe will be exposed after the HCR reaction, which can be used to assemble of multiple silver ions by C–Ag^+–C chelation [38]. Then, the Ag_2S can be generated in situ through the interaction between S^{2-} and Ag^+ ions, producing a desirable PEC signal. Because this approach does not require pre-synthesis of the photoactive material or direct modification of the photoactive material on the photoelectrode, the proposed ZBN PEC sensor is a convenient and sensitive method for the determination of OP molecules.

Experimental

Material and chemicals

Na_2S, $AgNO_3$ and Na_2SO_4 were supplied by Aladdin (Shanghai, China). $HAuCl_4 \cdot 3H_2O$ and malathion were acquired from Sigma-Aldrich (St. Louis, MO, USA). The apple juice samples including malathion were purchased from Kangtan Biotechnology Co. Ltd. (Guangdong, China). Deionized water (with a specific resistance of 18.2 MΩ cm at 25 °C) was obtained with a Milli-Q water purification system (Millipore SAS, France).

All the synthetic DNA utilized in all processes were products of Sangon Biotech Inc. (Shanghai, China). The detailed sequences of DNA are as follows:

S1: 5′-AAT TCG GGA GCC AAC ACC AGC ACA-3′
Aptamer: 5'-ATC CGT CAC ACC TGC TCT TAT ACA CAA TTG TTT TTC TCT TAA CTT CTT GAC TGC TGG TGT TGG CTC CCG TAT-3'
H1: 5'-CCC CCC CCC CCC TTA CGC CAC CTG GAG AAT TGC TGC TGG TGT TGG CTC CCG TGG GT-3'
H2: 5′-TGG GTC AAT TCT CCA GGT GGC GTT CGG GAG CCA ACA CCA GCA TCC CCC CCC CCC C-3'

Preparation of the PEC aptasensor for malathion

Firstly, a bare glassy carbon electrode (GCE) was repeatedly polished with 0.05 μm alumina slurry to obtain a completely clean surface, followed by sonication in anhydrous ethanol and deionized water alternately for 3 min [39]. After coating

with 5 μL Nafion ethanol solution (*v*/v, 2%), the Au was modified on the electrode surface by electrodeposition under an electric potential from −0.2 V to 1 V. Subsequently, the electrodes were washed with ultrapure water and dried in air. Then 10 μL of 1 μM S1 was incubated on the electrodes for 2 h at 37 °C. Next, 10 μL of 2 μM aptamer was dropped onto the electrodes to react at 37 °C for 1 h. After washing with ultrapure water, 10 μL of the malathion at different concentrations was incubated with the abovementioned mixture at 37 °C for 1 h. Malathion selectively combined with its aptamer, leading to the dissociation of the aptamer from the initiator strand. The above electrode reacted with the mixture containing 5 μL of 2.5 μM H1, 5 μL of 2.5 μM H2, and 5 μL of 4 mM $AgNO_3$ to trigger the HCR at 37 °C for 70 min, while a C–Ag^+–C chelation reaction occurred. Next, 15 μL of 10 μM Na_2S was added to the modified electrodes at room temperature for 5 min. During this process, the Ag_2S photoactive material was formed.

PEC measurement

After washing, the above electrode was immersed in 15 mL 0.1 M Na_2SO_4. The PEC measurement was carried out on a CHI 760E electrochemical workstation (CH Instruments, Shanghai, China), which was configured with a 500-W Xe lamp (NBET, Beijing, China) as the excitation light source under a constant potential of 1.0 V.

Results and discussion

The principle of the aptasensor

As shown in Scheme 1, a new type of photoelectrochemical sensor with near-zero background signal based on in situ generation of a Ag_2S photosensitive material and HCR nucleic acid signal amplification was designed for the detection of malathion. Firstly, S1 was fixed on the electrode surface by a Au–SH bond and then hybridized with the aptamer. After the addition of malathion, it was able to selectively bind with the aptamer and cause the exposure of S1. Subsequently, free S1 triggered the HCR in the presence of H1 and H2, resulting in the generation of DNA concatemers. Simultaneously, C–Ag^+–C chelation was formed with the addition of Ag^+. After that, the in situ-formed Ag_2S by the interaction of Ag^+ and S^{2-} presented a satisfactory signal to indicate the recognition of malathion.

Morphological characterization of Ag_2S

The successful synthesis of DNA-templated Ag_2S nanoparticles is critical for this strategy. To investigate the morphology of the as-synthesized Ag_2S nanoparticles, scanning electron microscopy (SEM) was used. In Fig. 1A, the SEM image shows that the Ag_2S nanoparticles formed were spherical, with an average diameter of 6–10 nm. The elemental composition of the Ag_2S nanoparticles was characterized using energy-dispersive spectrometry (EDS) (Fig. 1C), which confirmed that Ag, S and O were present in the nanostructures. In addition, the transmission electron microscopy (TEM) image of Ag_2S illustrates that the spherical nanoparticles were well distributed, with an average size of 7 nm. The high-resolution transmission electron microscopy (HRTEM) image shows a regular lattice fringe of 0.231 nm, which is in accord with the crystalline (−1, 0, 3) plane of Ag_2S (Fig. 1D) [40]. The results revealed that Ag_2S can be formed in situ through the interaction of S^{2-} and Ag^+ ions.

Evaluation of feasibility

The successful formation of HCR is essential for enhancing the performance of this PEC aptasensor. Therefore, as displayed in Fig. 2A, agarose gel electrophoresis was used to investigate the successful implementation of the HCR process. Lanes 1, 2, 3, and 4 represent the gel electrophoresis image of S1, H1, H2, and the mixture of H1 and H2, respectively. As indicated from lane 4, only one spot was observed. Therefore, it is obvious that the HCR cannot be processed without S1. When S1 was added to the mixture of H1 and H2 (lane 5), a typical bright band of HCR was obtained, indicating that the HCR process was successfully carried out.

Afterwards, the PEC signals in the presence and absence of the target malathion were recorded to further verify the feasibility of the HCR signal amplification strategy. Effectively, in the absence of a target molecule (curve a), HCR could not readily occur because S1 was covered by the aptamer [14]. Similarly, introduction of the target to the S1-aptamer DNA complex structure did not enhance the photocurrent of the sensor due to the lack of the C–Ag^+–C structure (curve b), which suppressed the growth of Ag_2S. In contrast, the photocurrent was strongly increased after the target-triggered HCR process was carried out (curve c). During the process, Ag_2S was formed in situ on the long DNA concatemer. Hence, these results validated the feasibility of this PEC aptasensor based on the in situ-formed Ag_2S photosensitive material and HCR signal amplification.

Photoelectrochemical and electrochemical characterization of the aptasensor

Photoelectrochemical characterization (PEC) was applied to measure the features of the step-by-step modified electrode. As indicated in Fig. 3A, no photocurrent signal was obtained at the bare GCE (curve a) [21]. When the electrode was modified stepwise by Au nanoparticles (NPs; curve b), S1 (curve c), aptamer (curve d), malathion (curve e), H1, H2, and Ag^+

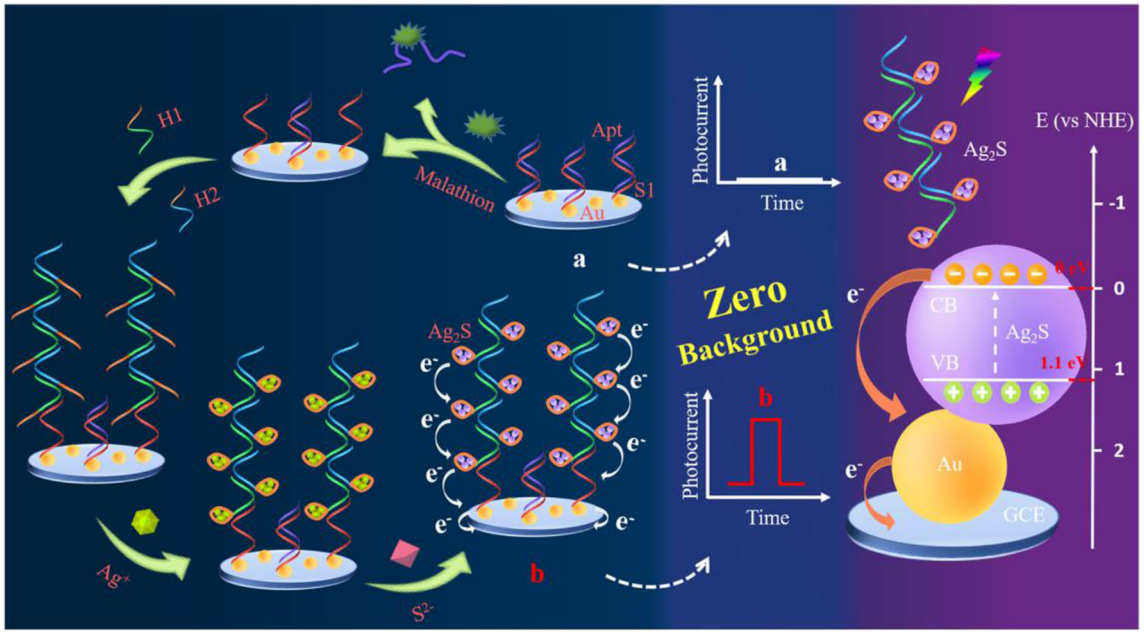

Scheme 1 Schematic illustration of the photoelectrochemical sensor based on HCR and in situ generation of a Ag_2S photosensitive material for the detection of malathion.

(curve f), there was still no photocurrent response. Upon the addition of S^{2-}, the in situ synthesis of Ag_2S NPs on the DNA concatemers obtained a strong photocurrent signal (curve g).

Electrochemical impedance spectroscopy (EIS) was employed to further characterize the gradual electron transfer on the electrode. The semicircle size on the Nyquist plot reflects the carrier transfer performance. Figure 3B shows that the charge transfer resistance (R_{ct}) value of the bare GCE is 201.6 Ω (curve a). After the electrode is modified by AuNPs, the R_{ct} value is decreased to 70.4 Ω (curve b), indicating that

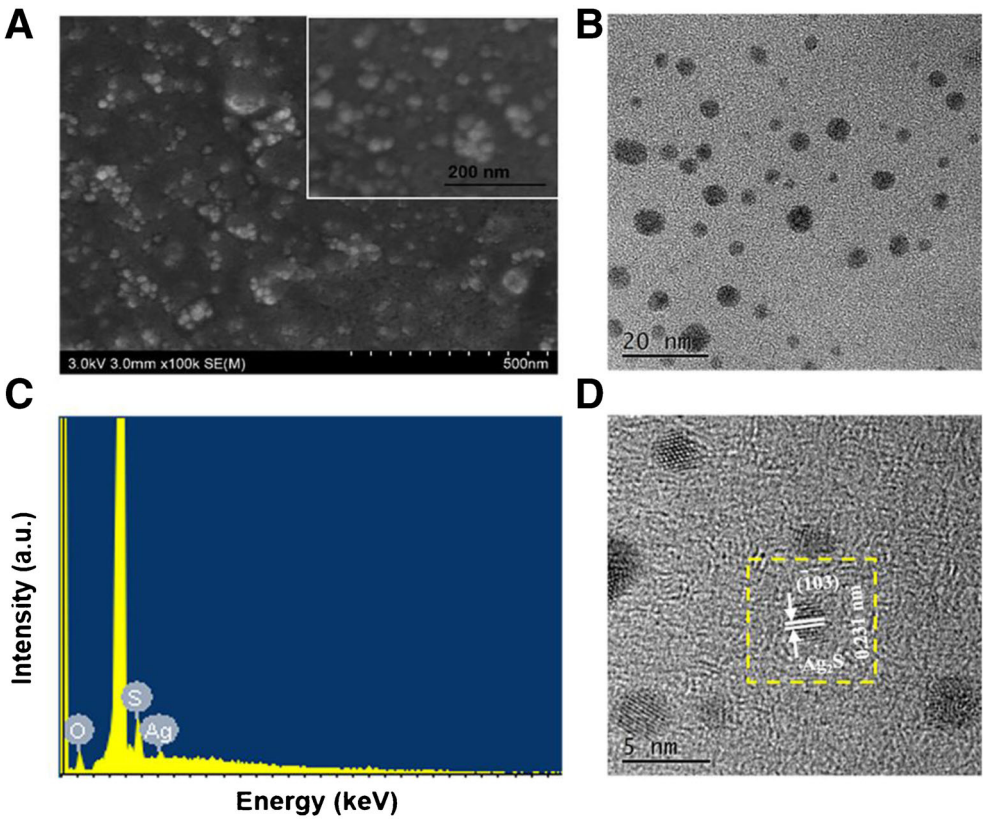

Fig. 1 (A) SEM image, (C) EDS image, (B) TEM image, and (D) HRTEM image of the in situ formation of Ag_2S by HCR

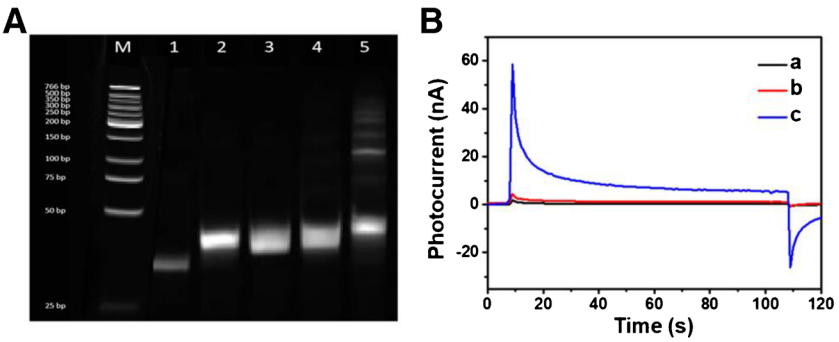

Fig. 2 (A) Agarose gel electrophoresis image (M: marker, lane 1: 2.0 μM S1, lane 2: 2.0 μM H1, lane 3: 2.0 μM H2, lane 4: 2.0 μM H1 and 2.0 μM H2, lane 5: 5.0 μM S1, 5.0 μM H1, and 5.0 μM H2); (B) photocurrent response in the absence of (a) malathion, and without (b) HCR and with (c) HCR in the presence of 6 ng mL^{-1} malathion

AuNPs have excellent electron transfer capability. The R_{ct} value is then increased to 89.5 Ω (curve c) with the modification of S1. When the electrode is incubated with the aptamer, the R_{ct} value of the electrode is further increased to 116.8 Ω (curve d) with the inhibition of electron transfer [41]. After the introduction of malathion, the R_{ct} value is decreased to 99.2 Ω because the target malathion combined selectively with the aptamer (curve e). Upon the addition of the mixture containing H1, H2, and Ag^+ to the electrode, the R_{ct} value is 105.1 Ω (curve f). Compared with curve d, the R_{ct} value of the electrode is decreased (curve f), which is attributed to the greatly improved electron transfer ability by Ag^+ [42]. Nevertheless,

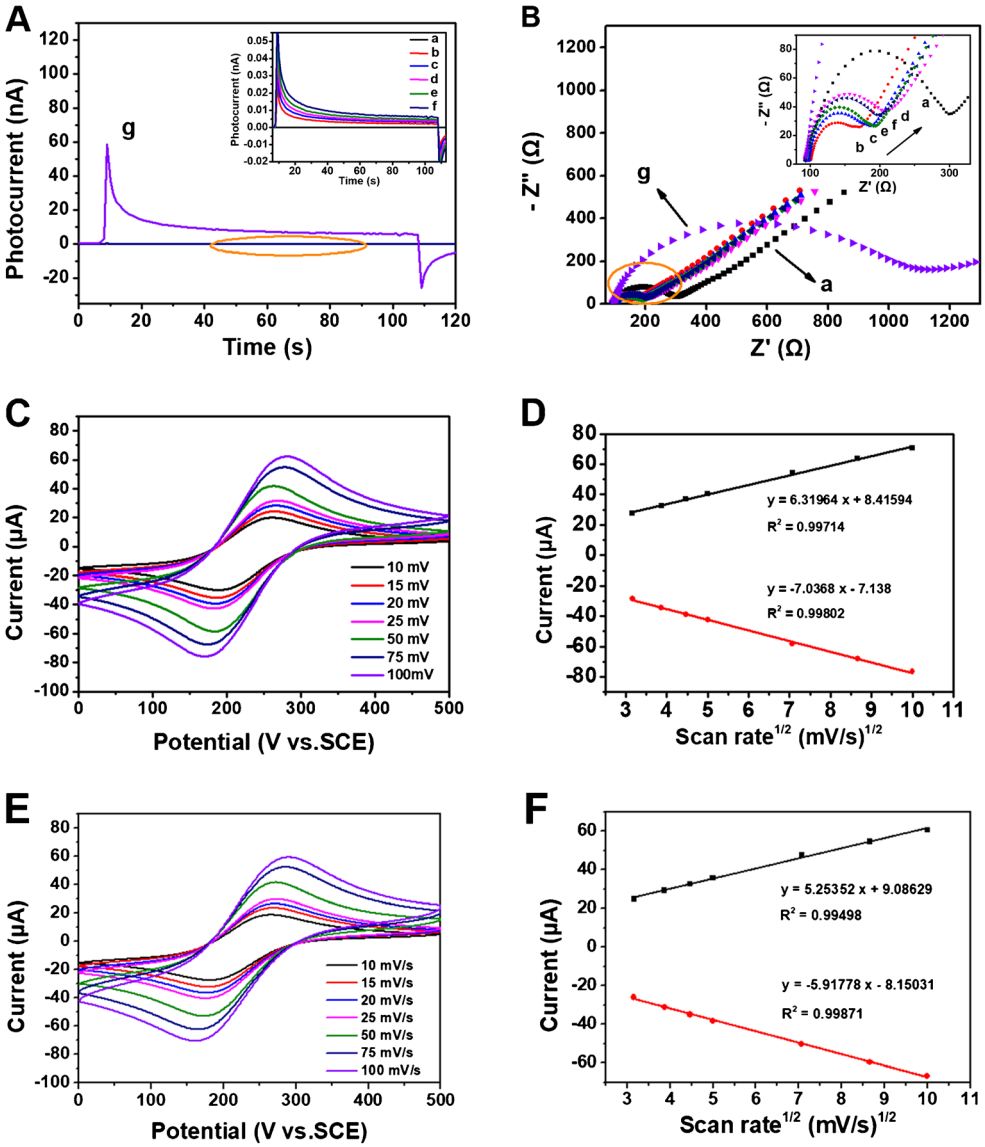

Fig. 3 PEC response (A) and EIS response (B) of (a) bare GCE, (b) AuNPs/GCE, (c) S1/AuNPs/GCE, (d) aptamer/S1/AuNPs/GCE, (e) malathion/aptamer/S1/AuNPs/GCE, (f) H1–H2–Ag^+/malathion/aptamer/S1/AuNPs/GCE, (g) S^{2-}/H1–H2–Ag^+/malathion/aptamer/S1/AuNPs/GCE. CVs of the bare GCE electrode (C) and Ag_2S-modified electrode (E). Peak current versus square root of the scan rate of the bare electrode (D) and modified electrode (F)

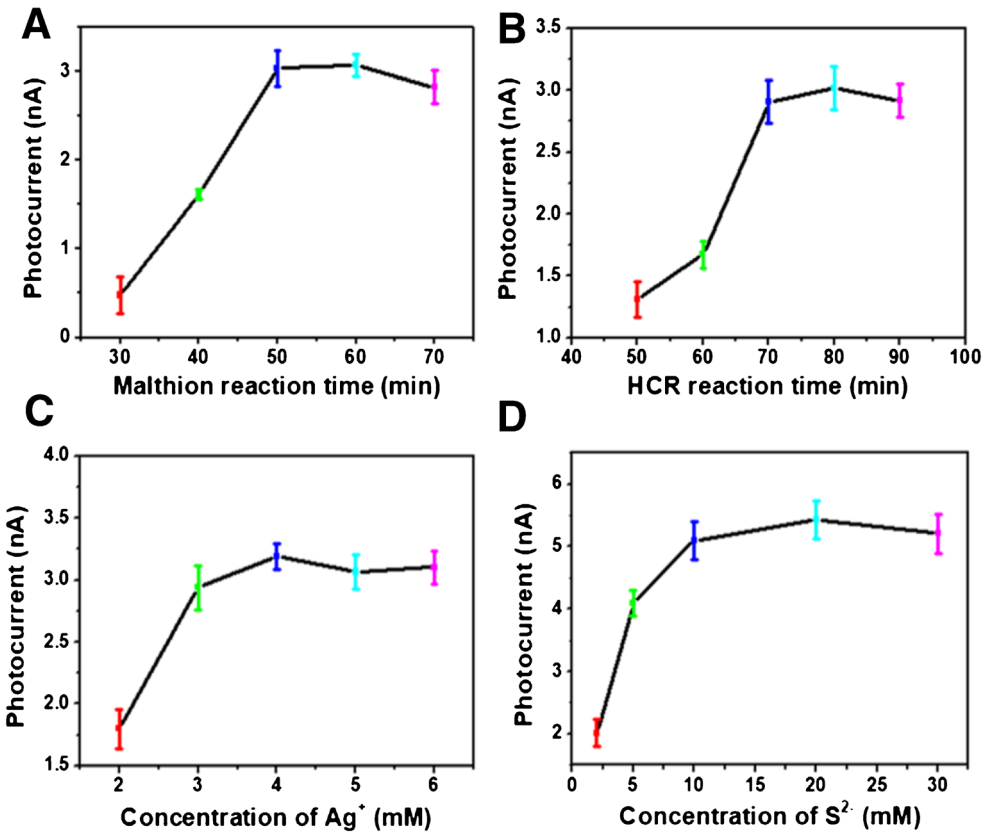

Fig. 4 Influence of (A) competitive reaction time between malathion and aptamer, (B) reaction time of HCR, (C) concentration of Ag^+, and (D) concentration of S^{2-} (6 ng mL^{-1} malathion utilized in these cases)

when S^{2-} is modified on the electrode, the R_{ct} value is dramatically increased to 1046.3 Ω (curve g) on account of the poor conductivity of the Ag_2S NPs. In short, the measurement results of EIS were highly consistent with those of PEC [32].

Additionally, cyclic voltammetry (CV) proved to be a reliable tool for the electrochemical characterization of the aptasensor. The CVs of a bare GCE electrode (Fig. 3C) and a modified GCE (Fig. 3E) were investigated at different scan rates in 0.1 M KCl containing 5.0 mM $[Fe(CN)_6]^{3-/4-}$. Significantly, when the electrode was modified with the Ag_2S NPs, the peak currents decreased and the peak-to-peak separation (ΔE_p) increased. In addition, the redox peak currents of the bare electrode (Fig. 3D) and the modified electrode (Fig. 3F) show a good linear relationship, with the square root of the scan rate in the range of 10–100 mV s^{-1}, thus illustrating that the redox reaction is a diffusion-controlled and quasi-reversible process. The electroactive area of the bare electrode and modified electrode were calculated using the Randles–Sevcik equation:

$$i_p = \left(2.69 \times 10^5\right) n^{2/3} A c D^{1/2} \upsilon^{1/2} \quad (1)$$

where i_p is the peak current, n is the electron transfer number, A is the electroactive area (cm^2), c is the analyte concentration,

Table 1 Comparison of assay performance between the developed sensing platform and other strategies

Probe	Linear range	Detection limit	Reference
Electrochemical Sensor	0.5–20 nM	0.3 nM	[44]
Electrochemical Sensor	0.89–5.94 and 5.94–44.6 nM	0.68 nM	[45]
Colorimetric Sensor	0.05–0.8 μM	11.8 nM	[46]
Electrochemical Sensor	0.1–100 nM	0.1 nM	[47]
Electrochemical Sensor	1–12 nM	0.1 nM	[48]
Electrochemical Sensor	Not reported	0.3 nM	[49]
Photoelectrochemical Sensor	0.006–600 ng mL^{-1} (0.018–1816.20 nM)	2 pg mL^{-1} (0.006 nM)	This work

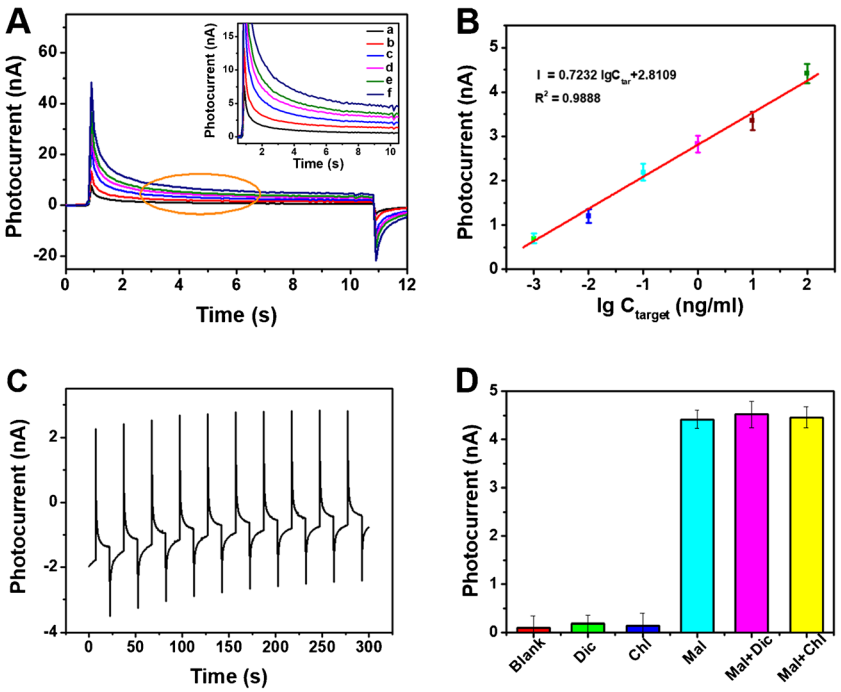

Fig. 5 (A) Photocurrent responses and (B) corresponding linear calibration curve of this PEC aptasensor at different concentrations of malathion (a–f: 0.006, 0.06, 0.6, 6, 60, 600 ng mL^{-1}); (C) the stability evaluation of malathion under periodic light for 10 cycles.; (D) specificity of the PEC aptasensor (malathion: 100 ng mL^{-1}, Dic and Chl: 2 mg mL^{-1})

D is the analyte diffusion coefficient (T = 298 K), 0.673 × 10^{-5} cm^{2}s^{-1}, and υ is the scan rate (V s^{-1}), 0.01 V s^{-1}. The calculated electroactive area of the bare electrode is 0.079 cm^2, and that of the modified electrode decreases to 0.071 cm^2.

The heterogeneous electron transfer (HET) rate constant (k^0) was estimated for the bare and modified electrodes via the Nicholson method. The estimated equation is displayed below [43]:

$$\Phi = k^0[\pi D n \upsilon F/(RT)]^{-1/2} \quad (2)$$

where Φ is the kinetic parameter, F is the Faraday constant, R is the universal gas constant, and T is the solution temperature. In addition, the kinetic parameter Φ is a function of ΔE_p, which relies on the following expression:

$$\Phi = (-0.628 + 0.0021X)/(1–0.017X) \quad (3)$$

where X = ΔE_p, the k^0 value of the bare electrode is 0.1662 cm s^{-1} and the value of the modified electrode decreases to 0.0957 cm s^{-1}. The results may be attributed to the poor conductivity of Ag_2S NPs, which corresponds to the above EIS data.

Optimization of experimental conditions

In order to obtain the optimal PEC aptasensor performance, several conditions were optimized, including the competitive reaction time between malathion and aptamer, HCR time, concentration of Ag^+, and concentration of S^{2-}.

First, the effect of competitive reaction time between malathion and the aptamer was monitored. Figure 4A shows that the photocurrent response increased gradually with the increase in the reaction time and reached its maximum value at 50 min. Therefore, 50 min was chosen as the optimized competitive reaction time. In addition, the PEC aptasensor performance largely depended on HCR. Thus, the reaction time of HCR was studied. Figure 4B shows that the response signal increased gradually with the reaction time and reached a stable level at 70 min due to the limitation of H1 and H2. A

Table 2 Results for detection of malathion in apple juice by the PEC aptasensor (n = 3)

Sample	Malathion (ng mL^{-1})	Added (ng mL^{-1})	Expected (ng mL^{-1})	Found (ng mL^{-1})	Recovery (%)	RSD (%)
1	130.14	0.06	130.20	130.197	95	2.94
2	130.14	0.6	130.74	130.73	98.3	1.39
3	130.14	6	136.14	135.90	96	2.16
4	130.14	60	190.14	192.21	103.5	1.27

Table 3 Comparison of the PEC method with gas chromatography for the determination of malathion in apple juice ($n = 3$)

Sample	GC method (ng mL^{-1})	PEC method (ng mL^{-1})	Student *t*-test
1	2 ± 0.06	1.98 ± 0.08	0.20
2	5 ± 0.05	5.06 ± 0.03	0.41
3	10 ± 0.08	10.13 ± 0.04	0.29
4	20 ± 0.04	20.27 ± 0.06	0.37
5	32.5 ± 0.02	32.83 ± 0.03	0.65
6	65 ± 0.02	65.55 ± 0.02	0.62
7	130 ± 0.01	130.14 ± 0.01	0.15

longer reaction time of HCR produced no further increase in the response signal. Therefore, in the interest of time, a reaction time of 70 min was applied as the optimal time for HCR.

The choice of the concentration of Ag^+ and S^{2-} was also crucial for the generation of Ag_2S. The results in Fig. 4C show that the maximum response signal was obtained at 4 mM Ag^+. Hence, 4 mM Ag^+ was used for fabricating the aptasensor. Figure 4D shows that the photocurrent signal increased gradually with an increase in the S^{2-} concentration from 2 mM to 10 mM. A further increase in the S^{2-} concentration yielded no significant enhancement in the photocurrent response, so 10 mM S^{2-} was adopted for the preparation of the assay.

Analytical performance

Under the optimal assay conditions, the PEC aptasensor was used for the detection of different concentrations of malathion. As can be seen from Fig. 5A, the photocurrent response increased stepwise with the increase in malathion concentration from 0.006 to 600 ng mL^{-1}. Figure 4B reveals that the photocurrent was proportional to the logarithm of malathion concentration in a dynamic range of 0.006–600 ng mL^{-1}, with a detection limit of 2 pg mL^{-1}. The linear regression equation was calculated to be $I = 0.7232\ lgC_{tar} + 2.8109$, with a reliable correlation coefficient of 0.9888. Moreover, the aptasensor exhibited a broader linear dynamic range and a lower detection limit than the values reported in previously published studies (Table 1).

The stability and specificity of the PEC aptasensor based on the in situ formation of Ag_2S NPs is critical to developing a new analytical strategy. As illustrated in Fig. 5C, the photocurrent signal was detected by repeatedly turning the lamp on and off 10 times. There was no significant change in the photocurrent, suggesting that the system had reliable stability. In addition, the specificity of this PEC aptasensor was detected by examining the system with non-target analytes including dichlorvos (Dic) and chlorpyrifos (Chl). As shown in Fig. 5D, the system did not respond to a high concentration (2 mg mL^{-1}) of non-target analytes. By contrast, the photocurrent signal of the mixture containing (100 ng mL^{-1}) malathion and non-target analytes was similar to malathion alone, indicating the excellent specificity of this PEC aptasensor for malathion.

Recovery measurement

The practicability of the PEC aptasensor was investigated in apple juice samples using the standard addition method. First, the malathion concentration in the original apple juice samples was detected using this PEC aptasensor. Following that, various concentrations of standard malathion (0.06, 0.6, 6, 60 ng mL^{-1}) were added to these samples to measure the corresponding photocurrent by the PEC method. The recovery was calculated according to the following equation [50]:

$$\text{Recovery}\ (\%) = \left(\frac{C1-C2}{C3}\right) \times 100 \quad (4)$$

where C1 is the final concentration, C2 is the initial concentration and C3 is the added concentration.

It can be observed from Table 2 that the recoveries of malathion were within a range of 95–103.5% and the relative standard deviation (RSD) varied from 1.27 to 2.94%.

In addition, the photocurrent signal of different amounts of malathion in apple juice was measured by a reference gas chromatography method and the developed PEC aptasensor method. A comparison of the results in Table 3 shows a Student *t*-test value of between 0.15 and 0.65, revealing the excellent reliability of this system.

Conclusions

In conclusion, by coupling of HCR-promoted in situ generation of photoactive materials, a sensitive signal-on ZBN PEC biosensor was developed for determination of malathion. The target molecule hybridized with the aptamer molecule and triggered the HCR reaction to generate a long dsDNA polymer containing multiple "C" strands. The long dsDNA concatemer was employed to load silver ions by the terminated C-rich strands. After treatment with S^{2-}, a large number of Ag_2S were generated on the long dsDNA concatemer, producing impressive photocurrent response. Benefiting from the ZBN and HCR signal amplification strategy, the proposed PEC biosensor displayed a wide linear range, low detection limit, and excellent selectivity. Therefore, this concept offers a new analytical strategy for developing ZBN signal-on PEC and provides a powerful tool in the field of food safety testing.

Acknowledgements This work was financially supported by the National Natural Science Foundation of China (21864013), the Science Foundation for Excellent Young Scholars of Jiangxi Province (20202ZDB01003), the Natural Science Foundation of Jiangxi Province

(20202BAB203008), and the Postdoctoral Science Foundation of Jiangxi Province (2019KY40).

Declarations

Conflict of interest The authors declare no competing interests.

References

1. Yao T, Liu A, Liu Y, Wei M, Wei W, Liu S. Ratiometric fluorescence sensor for organophosphorus pesticide detection based on opposite responses of two fluorescence reagents to MnO_2 nanosheets. Biosens Bioelectron. 2019;145:111705.
2. Zhang J, Fang X, Wu J, Hu Z, Jiang Y, Qi H, et al. An interdigitated microelectrode based aptasensor for real-time and ultratrace detection of four organophosphorus pesticides. Biosens Bioelectron. 2019;150:111879.
3. Li J, Xiong P, Tang J, Liu L, Gao S, Zeng Z, et al. Biocatalysis-induced formation of $BiOBr/Bi_2S_3$ semiconductor heterostructures: a highly efficient strategy for establishing sensitive photoelectrochemical sensing system for organophosphorus pesticide detection. Sens Actuators B Chem. 2021;331:129451.
4. Long Q, Li H, Zhang Y, Yao S. Upconversion nanoparticle-based fluorescence resonance energy transfer assay for organophosphorus pesticides. Biosens Bioelectron. 2015;68:168–74.
5. Chen J, Chen X, Zhao J, Liu S, Chi Z. Instrument-free and visual detection of organophosphorus pesticide using a smartphone by coupling aggregation-induced emission nanoparticle and two-dimension MnO_2 nanoflake. Biosens Bioelectron. 2020;170:112668.
6. Zhang SX, Xue SF, Deng J, Zhang M, Shi G, Zhou T. Polyacrylic acid-coated cerium oxide nanoparticles: an oxidase mimic applied for colorimetric assay to organophosphorus pesticides. Biosens Bioelectron. 2016;85:457–63.
7. Wang J, Chow W, Leung D, Chang J. Application of ultrahigh-performance liquid chromatography and electrospray ionization quadrupole orbitrap high-resolution mass spectrometry for determination of 166 pesticides in fruits and vegetables. J Agric Food Chem. 2012;60(49):12088–104.
8. Cacho JI, Campillo N, Vinas P, Hernandez-Cordoba M. In situ ionic liquid dispersive liquid-liquid microextraction coupled to gas chromatography-mass spectrometry for the determination of organophosphorus pesticides. J Chromatogr A. 2018;1559:95–101.
9. Yao C, Cheng F, Wang C, Wang Y, Guo X, Gong Z, et al. Separation, identification and fast determination of organophosphate pesticide methidathion in tea leaves by thin layer chromatography–surface-enhanced Raman scattering. Anal Methods. 2013;5(20):5560–4.
10. Olsson AO, Baker SE, Nguyen JV, Romanoff LC, Udunka SO, Walker RD, et al. A liquid chromatography−tandem mass spectrometry multiresidue method for quantification of specific metabolites of Organophosphorus pesticides, synthetic Pyrethroids, selected herbicides, and DEET in human urine. Anal Chem. 2004;76(9):2453–61.
11. Liu Y, Yan K, Zhang J. Graphitic carbon nitride sensitized with CdS quantum dots for visible-light-driven Photoelectrochemical Aptasensing of tetracycline. ACS Appl Mater Interfaces. 2016;8(42):28255–64.
12. Zhang L, Shen YL, Fan GC, Xiong M, Yu XD, Zhao WW. Preparation of an $AgI/CuBi_2O_4$ heterojunction on a fluorine-doped tin oxide electrode for cathodic photoelectrochemical assays: application to the detection of L-cysteine. Mikrochim Acta. 2019;186(5):284.
13. Shu J, Tang D. Recent advances in Photoelectrochemical sensing: from engineered photoactive materials to sensing devices and detection modes. Anal Chem. 2020;92(1):363–77.
14. Tang J, Li J, Xiong P, Sun Y, Zeng Z, Tian X, et al. Rolling circle amplification promoted magneto-controlled photoelectrochemical biosensor for organophosphorus pesticides based on dissolution of core-shell MnO_2 nanoflower@CdS mediated by butyrylcholinesterase. Mikrochim Acta. 2020;187(8):450.
15. Hao N, Hua R, Chen S, Zhang Y, Zhou Z, Qian J, et al. Multiple signal-amplification via Ag and TiO_2 decorated 3D nitrogen doped graphene hydrogel for fabricating sensitive label-free photoelectrochemical thrombin aptasensor. Biosens Bioelectron. 2018;101:14–20.
16. Li J, Yin O, Zhao L, Wang Z, Dong B, Wan L, et al. Enhancing the photoelectric conversion efficiency of dye-sensitized solar cell using the upconversion luminescence materials $Y_2O_3:Er^{3+}$ nanorods doped TiO_2 photoanode. Materials Letters. 2018;227:209–12.
17. Qian Y, Feng J, Xu R, Fan D, Du Y, Ren X, et al. Zinc and molybdenum co-doped $BiVO_4$ Nanoarray for Photoelectrochemical diethylstilbestrol analysis based on the dual-competitive system of manganese Hexacyanoferrate hydrate Nanocubes. ACS Appl Mater Interfaces. 2020;12(14):16662–9.
18. Tayebi M, Tayyebi A, Masoumi Z, Lee B-K. Photocorrosion suppression and photoelectrochemical (PEC) enhancement of ZnO via hybridization with graphene nanosheets. Applied Surface Science. 2020;502:144189.
19. Yang X, Zhang M, Chen Z, Bu Y, Gao X, Sui Y, et al. Sodium alginate micelle-encapsulating zinc Phthalocyanine dye-sensitized Photoelectrochemical biosensor with CdS as the photoelectric material for Hg^{2+} detection. ACS Appl Mater Interfaces. 2021;13(14):16828–36.
20. Tang J, Cheng Y, Zheng J, Li J, Sun Y, Peng S, et al. Target-engineered photo-responsive DNA strands: a novel signal-on photoelectrochemical biosensing platform for ochratoxin a. Anal Methods. 2019;11(43):5638–44.
21. Da H, Liu H, Zheng Y, Yuan R, Chai Y. A highly sensitive VEGF165 photoelectrochemical biosensor fabricated by assembly of aptamer bridged DNA networks. Biosens Bioelectron. 2018;101:213–8.
22. Da H, Liu Y, Li M, Yuan R, Liu H, Chai Y. A highly sensitive photoelectrochemical VEGF165 biosensor with a dual signal amplification strategy by using $AgVO_3$ as a photoactive material. Chem Commun. 2019;55(56):8076–8.
23. Xiao K, Meng L, Du C, Zhang Q, Yu Q, Zhang X, et al. A label-free photoelectrochemical biosensor with near-zero-background noise for protein kinase a activity assay based on porous ZrO_2/CdS octahedra. Sens Actuators B Chem. 2021;328:129096.
24. Li M, Xiong C, Zheng Y, Liang W, Yuan R, Chai Y. Ultrasensitive Photoelectrochemical biosensor based on DNA tetrahedron as Nanocarrier for efficient immobilization of CdTe QDs-methylene blue as signal probe with near-zero background noise. Anal Chem. 2018;90(13):8211–6.
25. Shen H, Jiao X, Oron D, Li J, Lin H. Efficient electron injection in non-toxic silver sulfide (Ag_2S) sensitized solar cells. Journal of Power Sources. 2013;240:8–13.
26. Li R, Tu W, Wang H, Dai Z. Near-infrared light excited and localized surface Plasmon resonance-enhanced Photoelectrochemical biosensing platform for cell analysis. Anal Chem. 2018;90(15):9403–9.
27. Mirahmadi FS, Marandi M, Karimipour M, Molaei M. Microwave activated synthesis of Ag_2S and Ag_2S@ZnS nanocrystals and their application in well-performing quantum dot sensitized solar cells. Sol Energy. 2020;202:155–63.
28. Kozhevnikova NS, Vorokh AS, Shalaeva EV, Baklanova IV, Tyutyunnik AP, Zubkov VG, et al. One-pot inorganic route to

highly stable water-dispersible Ag_2S quantum dots. J Alloys and Compd. 2017;712:418–24.
29. Lu F, Ju W, Zhao N, Zhao T, Zhan C, Wang Q, et al. Aqueous synthesis of PEGylated Ag_2S quantum dots and their in vivo tumor targeting behavior. Biochem Biophys Res Commun. 2020;529(4):930–5.
30. Liu D, Lai J, Wang R, Ye L, Tian Y. Reverse microemulsion synthesis of Fe_3O_4–Ag_2S Heteronanocrystals for dual-modal imaging-guided Photothermal tumor ablation. ACS Biomater Sci Eng. 2019;5(11):6196–206.
31. Zhai LY, Li MX, Pan WL, Chen Y, Li MM, Pang JX, et al. In situ detection of plasma Exosomal MicroRNA-1246 for breast Cancer diagnostics by a au Nanoflare probe. ACS Appl Mater Interfaces. 2018;10(46):39478–86.
32. Yuan Y, Hu T, Zhong X, Zhu M, Chai Y, Yuan R. Highly sensitive Photoelectrochemical biosensor based on quantum dots sensitizing Bi_2Te_3 Nanosheets and DNA-amplifying strategies. ACS Appl Mater Interfaces. 2020;12(20):22624–9.
33. Yu X, Zhang ZL, Zheng SY. Highly sensitive DNA detection using cascade amplification strategy based on hybridization chain reaction and enzyme-induced metallization. Biosens Bioelectron. 2015;66:520–6.
34. Yao GH, Liang RP, Yu XD, Huang CF, Zhang L, Qiu JD. Target-triggering multiple-cycle amplification strategy for ultrasensitive detection of adenosine based on surface plasma resonance techniques. Anal Chem. 2015;87(2):929–36.
35. Guo J, Wang J, Zhao J, Guo Z, Zhang Y. Ultrasensitive multiplexed immunoassay for tumor biomarkers based on DNA hybridization chain reaction amplifying signal. ACS Appl Mater Interfaces. 2016;8(11):6898–904.
36. Lu L, Wang J, Miao W, Wang X, Guo G. Electrogenerated Chemiluminescence biosensor with a tripod probe for the highly sensitive detection of MicroRNA. Anal Chem. 2019;91(2):1452–9.
37. Li H, Wang J, Wang X, Lin H, Li F. Perylene-based photoactive material as a double-stranded DNA intercalating probe for ultrasensitive Photoelectrochemical biosensing. ACS Appl Mater Interfaces. 2019;11(18):16958–64.
38. Qiu Z, Shu J, Tang D. $NaYF_4$:Yb,Er Upconversion Nanotransducer with in Situ Fabrication of Ag_2S for Near-Infrared Light Responsive Photoelectrochemical Biosensor. Anal Chem. 2018;90(20):12214–20.
39. Sun Y, Xiong P, Tang J, Zeng Z, Tang D. Ultrasensitive split-type electrochemical sensing platform for sensitive determination of organophosphorus pesticides based on MnO_2 nanoflower-electron mediator as a signal transduction system. Anal Bioanal Chem. 2020;412(25):6939–45.
40. Zhang S, Wang J, Chen S, Li R, Peng T. Construction of Ag_2S/WO_3 direct Z-scheme Photocatalyst for enhanced charge separation efficiency and H_2 generation activity. Ind Eng Chem Res. 2019;58(32):14802–13.
41. Ge S, Lan F, Liang L, Ren N, Li L, Liu H, et al. Ultrasensitive Photoelectrochemical biosensing of cell surface N-glycan expression based on the enhancement of Nanogold-assembled Mesoporous silica amplified by Graphene quantum dots and hybridization chain reaction. ACS Appl Mater Interfaces. 2017;9(8):6670–8.
42. He Z-J, Kang T-F, Lu L-P, Cheng S-Y. An electrochemiluminescence aptamer sensor for chloramphenicol based on GO-QDs nanocomposites and enzyme-linked aptamers. J Electroanal Chem. 2020;860:113870.
43. Thakur B, Bernalte E, Smith J, Linton P, Sawant S, Banks C, et al. The Mediatorless Electroanalytical sensing of sulfide utilizing unmodified graphitic electrode materials. C. 2016;2(2):14.
44. Rodrigues NFM, Neto SY, Luz RCS, Damos FS, Yamanaka H. Ultrasensitive determination of Malathion using Acetylcholinesterase immobilized on chitosan-functionalized magnetic Iron nanoparticles. Biosensors (Basel). 2018;8(1):16.
45. Bolat G, Abaci S. Non-enzymatic electrochemical sensing of Malathion pesticide in tomato and apple samples based on gold nanoparticles-chitosan-ionic liquid hybrid Nanocomposite. Sensors (Basel). 2018;18(3):773.
46. Li D, Wang S, Wang L, Zhang H, Hu J. A simple colorimetric probe based on anti-aggregation of AuNPs for rapid and sensitive detection of malathion in environmental samples. Anal Bioanal Chem. 2019;411(12):2645–52.
47. Chauhan N, Narang J, Pundir CS. Immobilization of rat brain acetylcholinesterase on porous gold-nanoparticle-$CaCO_3$ hybrid material modified au electrode for detection of organophosphorous insecticides. Int J Biol Macromol. 2011;49(5):923–9.
48. Soomro RA, Hallam KR, Ibupoto ZH, Tahira A, Sherazi STH, Sirajjuddin MSS, et al. Amino acid assisted growth of CuO nanostructures and their potential application in electrochemical sensing of organophosphate pesticide. Electrochim Acta. 2016;190:972–9.
49. Huo D, Li Q, Zhang Y, Hou C, Lei Y. A highly efficient organophosphorus pesticides sensor based on CuO nanowires–SWCNTs hybrid nanocomposite. Sens Actuators B Chem. 2014;199:410–7.
50. Antunes R, Ferraz D, Garcia L, Thomaz D, Luque R, Lobón G, Gil E, Lopes F. Development of a polyphenol oxidase biosensor from Jenipapo fruit extract (*Genipa americana* L.) and determination of phenolic compounds in textile industrial effluents. Biosensors (Basel). 2018;8(2):47.